

We are IntechOpen, the world's leading publisher of Open Access books Built by scientists, for scientists

6,900

Open access books available

186,000

International authors and editors

200M

Downloads

Our authors are among the

154

Countries delivered to

TOP 1%

most cited scientists

12.2%

Contributors from top 500 universities



WEB OF SCIENCE™

Selection of our books indexed in the Book Citation Index
in Web of Science™ Core Collection (BKCI)

Interested in publishing with us?
Contact book.department@intechopen.com

Numbers displayed above are based on latest data collected.
For more information visit www.intechopen.com



Time-Domain Analysis of Modified Vivaldi Antennas

Sultan Aldırmaz Çolak and Nurhan Türker Tokan

Additional information is available at the end of the chapter

<http://dx.doi.org/10.5772/intechopen.74945>

Abstract

In the ultra-wideband (UWB) application frequency domain parameters such as gain, group delay isn't sufficient to demonstrate the performance of the antenna. Besides frequency domain analysis, a time-domain analysis is required to characterize the transient behavior of UWB antennas for pulsed operations since pulse distortion of the UWB antenna reduces the system performance and decreases the signal to noise ratio (SNR) of the UWB communication system. Vivaldi antenna is a widely used UWB antenna, especially in microwave imaging applications. Performance of Vivaldi antennas is enhanced by adding corrugation on the edge of exponential flaring and/or grating elements on the slot area. From the measured scattering parameters of modified Vivaldi antennas, pulse preserving capabilities are observed. Pulse width extension and fidelity factor parameters are used to define the similarity between the transmitted and received pulse. The analysis is performed with angular dependence with respect to the signal transmitted at the main beam direction.

Keywords: UWB antenna, Vivaldi antenna, time domain, pulse distortion, fidelity analysis, corrugation

1. Introduction

Ultra-wideband (UWB) systems have been used in various applications that range from deep space investigation to commercial telecommunication links and radars with high spatial resolutions [1–3]. Due to its low complexity, small physical size, low manufacturing cost, low interference and high time-domain resolution, it is widely used in communication systems, microwave imaging, remote sensing and radar.

In 2012, federal communications commission (FCC) has allocated 7.5 GHz-wide frequency band that ranges from 3.1 to 10.6 GHz for UWB applications [4]. In UWB systems, antennas

can be considered as the key component that affects the system performance. The performance and quality of UWB antennas are mostly analyzed in the frequency domain. For narrow-band systems, traditional frequency domain parameters (such as gain, group delay time, etc.) are enough to assess the performance of the antenna. However, in the ultra-wideband applications, these parameters are not sufficient to demonstrate the performance of the antenna. Besides frequency domain analysis, a time-domain analysis is required to characterize the transient behavior of UWB antennas for pulsed operations [5]. The antenna's transient response is the quantity for the characterization of the signal distortion and correlation of the radiated pulse in the time domain [6–7]. The time-dispersion characteristic of the antenna is one of the most important factors that should be considered in ultra-wideband applications since antennas with smaller time dispersion will have a better energy-focusing property and anti-interference performance. Antenna with larger dispersion leads to a less stable phase center and increases the interference in UWB communications based on pulse radio [8]. Consequently, this will result in time spreading of pulses and make signal transmission less predictable and less reliable in sensor system. Thus, it is necessary to investigate the antenna and radio propagation performance. This analysis should be performed not only in the main beam direction of the antenna but also in an arbitrary angular direction. By calculating the correlation between the transmitted signal and radiated signal in an arbitrary angular direction, the angular region where the pulse is preserved can be determined.

In order to radiate a short pulse with low distortion, the antenna needs to efficiently operate over a broad bandwidth and be non-dispersive, with a stable phase center at all frequencies. One of the most widely employed solutions for broadband planar, directive antenna is tapered slot antenna. With its relatively small physical size, low cost, easy integration with the circuit board and almost stable radiation properties within its band, exponentially tapered slot antenna, which is also known as Vivaldi antenna, became a good candidate for UWB communication, radar and microwave imaging applications [9–10]. Recent works have aimed to increase its radiation performance by physically modifying its structure. A parasitic elliptical patch is inserted in the slot aperture for radiation stability and directivity improvement at high frequencies [11]. In [12], to reduce side- and back-lobe levels, extend the bandwidth and increase the main lobe gain, an exponential slot edge is added to the structure. In [13], a double slot structure is proposed in the Vivaldi antenna, to enhance the directivity and radiation performance, whereas double antipodal structure having corrugated edges and the semicircle director is presented in [14] for the same purpose. Vivaldi antenna is modified by incorporating corrugations on the edges of the exponential tapered slots and periodic grating elements consisting of metallic strips on the slot area in [15] to increase gain, especially at the lower end of the frequency band.

Time-domain characteristics of standard Vivaldi antennas are investigated and proved to be weakly dispersive in [16]. In [17], the time-domain radiation properties of the Vivaldi antenna are analyzed with angular dependence with respect to the signal transmitted at the main beam direction. In literature, time-domain characteristics of the modified Vivaldi antennas are not considered so far. With this work, effects of the physical modification on the Vivaldi structure will be observed in the time domain. If the modifications made to improve frequency-domain parameters would benefit time-domain parameters, they will be investigated, and potentials of these antennas to be used as basic element for non-distorted radiated link are discussed.

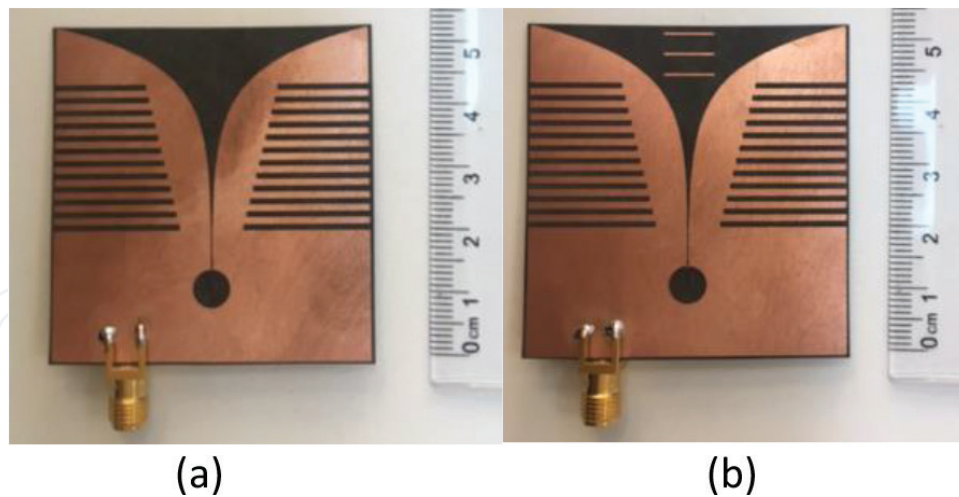


Figure 1. Modified Vivaldi antennas with (a) corrugation and (b) corrugation and strip.

Pulse-preserving capabilities of modified Vivaldi antennas given in **Figure 1** are measured in terms of two parameters: the pulse width extension and the fidelity factor. In addition, the results are compared with that of the standard Vivaldi antennas. Their time-domain performance is quantified by their respective standard deviations from the width of the ideal signal that has constant value. Standard Fourier transform relationship is used to recover time-domain waveforms. Although this chapter concentrates on Vivaldi structures operating in 3.1–10.6 GHz, the analysis is also applicable to any UWB antenna.

This chapter is organized as follows: In the next Section, time-domain analysis and the procedure for the analysis of the angular distortion of radiated pulses are presented. In Section 3, the modified Vivaldi antennas are introduced and their frequency-domain performance is demonstrated. Measurement setup and time-domain analysis results of the antennas are given in Section 4. Section 5 concludes the whole chapter.

2. Time-domain analysis

Despite the wide frequency of the radiation, the transmitted UWB waveform is dispersive. This is one major difference from narrow-band circumstances. When the signal is transmitted through a UWB antenna, the antenna output signal contains the input signal and its derivatives with varying delays, caused mainly by the resonances in the radiator structure. Frequency-dependent variations of antenna characteristics and reflection coefficients, and RF circuitry, are considered as the sources of waveform dispersion [18]. When s_{21} parameter of the link in the frequency domain presents linear phase variation which results as non-dispersive radiation and constant amplitude which results as no amplitude distortion, the time-domain pulse is not distorted.

Impulse response of a link, $S_{21}(t, \theta, \varphi)$, can be derived by taking the inverse Fourier transform of $S_{21}(\omega, \theta, \varphi)$:

$$S_{21}(t, \theta, \varphi) = IFT \{S_{21}(\omega, \theta, \varphi)\} \quad (1)$$

where the angle θ starts from the positive z -axis and the angle ϕ starts from the positive x -axis. ω refers to angular frequency, whereas t denotes time. Pulse distortion in the time domain can be observed from the difference between the received and transmitted UWB pulse in shape.

2.1. Time-domain parameters

The main parameters for the evaluation of the pulse characteristics in the time domain are obtained from the transient response of the antenna [5]. The peak value of the antenna impulse response, $P(\theta, \varphi)$, is expressed in Eq. (2):

$$P(\theta, \varphi) = \max |S_{21}(t, \theta, \varphi)| \quad (2)$$

The angular dependency of P is the result of angular-dependent impulse response. Most energy is contained around the peak of the impulse response. The higher values of $P(\theta, \varphi)$ demonstrates lower loss of the link. The pulse width is the width of the time window that contains a certain percentage of the total energy. Half-power width, τ , is a parameter used to define the broadening of the signal:

$$\tau = t_2 \Big|_{|S_{21}(t, \theta, \varphi)|=0.7 P_{nor,max}(\theta, \varphi)} - t_1 \Big|_{t_1 < t_2, |S_{21}(t, \theta, \varphi)|=0.7 P_{nor,max}(\theta, \varphi)} \quad (3)$$

where $P_{nor,max}$ is the maximum value of the normalized version of the antenna impulse response. t_2 and t_1 are the instants when half power width occurs, after and before the maximum, respectively. Time difference between the half power width of the received signal and the reference signal describes the broadening of the transmitted pulse. Thus, when there is no distortion, τ of the received pulse is equal to the τ of the transmitted pulse. This is the ideal case. However, mostly the link is distorted and the widening affects the communication quality. Ringing duration parameter, τ_r given in Eq. (4), defines the oscillations in the antenna impulse response:

$$\tau_r = t_r \Big|_{|S_{21}(t, \theta, \varphi)|=RP(\theta, \varphi)} - t_p \Big|_{t_r < t_p, |S_{21}(t, \theta, \varphi)|=P(\theta, \varphi)} \quad (4)$$

R is a coefficient that is used to define the instant of the ringing. t_p and t_r are the instants when the pulse has its maximum and first ringing, respectively. Although these parameters are widely used to quantify the time-domain signal, correlation between the transmitted and received pulse should be observed as well. Besides, due to the angular variation of the transmitted signal, cross-correlation between the transmitted and received signals should be investigated and quantified not only at the main beam direction but also with angular dependence as given in [19].

2.2. Fidelity analysis

The correlation coefficient between the received pulse and transmitted pulse demonstrates the amount of pulse distortion which the antenna induced. The fidelity factor, FF , is a parameter used to quantify the similarity between transmitted and received signal [16]:

$$FF = \max_{\tau} \frac{\int_{-\infty}^{+\infty} S_{ref}(t) S_{21}(t - \tau) dt}{\sqrt{\int_{-\infty}^{+\infty} |S_{ref}(t)|^2 dt} \sqrt{\int_{-\infty}^{+\infty} |S_{21}(t)|^2 dt}} \quad (5)$$

where $S_{ref}(t)$ and $S_{21}(t)$ are the transmitted and received signals, respectively. If the transmitted and received signals are exactly same, FF coefficient has its maximum of 1. When FF coefficient is 1, input signal isn't distorted by the antenna. Fidelity depends on the spatial radiation characteristics of the antenna. Thus, angular variation of the FF coefficient should also be observed. Because of the normalization procedure, fidelity factor cannot provide information about the amplitudes of signals.

3. Modified Vivaldi antennas

3.1. Antenna design

The Vivaldi antenna is one of the classical ultra-wideband antennas with many applications [8]. It is a traveling-wave, end-fire antenna and due to its completely planar structure, it can be easily integrated in UWB sensor circuit. It has almost symmetric radiation patterns in the E and H planes. Theoretically, with its exponentially tapered slot, the Vivaldi antenna has an unlimited range of operating frequencies. However, in practice, it is constrained by the physical dimensions such as taper dimensions, the slot line width and transition from the feed line.

The structure of the standard Vivaldi antenna together with its dimensions is shown in **Figure 2a**. The proposed Vivaldi antenna consists of a microstrip feed line, microstrip line to slot line transition and the radiating structure. It is designed to operate efficiently as the transmitter and receiver in the unlicensed band of 3.1–10.6 GHz (7.5 GHz bandwidth). The slot curve of the Vivaldi antenna is the exponential function, which is expressed as $S(z) = (W_{slot}/2) e^{az}$ where $a = 0.165$ and $W_{slot} = 0.25$ mm. A quarter wavelength open circuit stub is used for wideband matching. The aperture coupling is optimized for the frequency range from 3.1 to 10.6 GHz. The size of the Vivaldi antenna is 50×50 mm. Its dimensions are given in **Figure 2a**. Rogers RT/Duroid 5870 with 0.51-mm dielectric thickness and 17.5- μ m copper is chosen for the design. The dielectric constant of the dielectric material is $\epsilon_r = 2.33$.

One of the bottlenecks of the conventional Vivaldi antenna is its relatively low directivity, especially at lower frequencies of the band. The lower frequency response of Vivaldi antennas with satisfactory impedance match and effective radiation is usually improved by increasing the aperture size. Another solution is introducing variable length slots to effectively increase the aperture of the antenna [15, 20]. It is shown that by incorporating a corrugated profile on the sides of exponential flaring, more suitable characteristics, especially for microwave imaging applications (i.e., higher gain, broader bandwidth), can be obtained compared to standard Vivaldi designs [21].

Performance of these antennas is widely discussed in the frequency domain. Time-domain analysis of these antennas is also needed since these antennas are considered as a good choice for microwave imaging applications [21]. With this aim, Vivaldi antenna with corrugations is designed to operate at UWB frequencies. It has the same size and uses the same material as

the standard Vivaldi. The dimensions of the Vivaldi with corrugations are given in **Figure 2b**. The edge of Vivaldi is symmetrically corrugated by slots along the y -axis. The corrugations are rectangular slots with varying lengths. Design parameters of the corrugations are the distance between slots, the width of slots and the length of slots. The width of slots and distance between the rectangular slots of corrugation remain same. The length of the slots decreases gradually toward the flaring. Simulations proved that increasing the number of slots improves the radiation characteristics of the designed antenna by triggering extra resonances and modifying the direction of the current on the edges. The corrugations on the edges of the flaring act like a resistive loading. These corrugations are useful to concentrate the wave toward the slot area and contribute to the end-fire radiation patterns. The design parameters of the corrugation are optimized as 1 mm, 1 and 20–14.5 mm, respectively.

Besides adding corrugations on the edges of the flaring, adding grating elements on the slot area in the direction of the antenna axis is another technique to enhance the gain of the antenna. These elements work as directive elements and contribute to the radiation in the end-fire direction. With the combination of both the corrugations and grating elements, the gain of the antenna increases significantly in the end-fire direction [15].

The third design for the Vivaldi antennae is achieved by adding three metallic strips on the slot area as demonstrated in **Figure 2c**. Design parameters of the grating elements that are

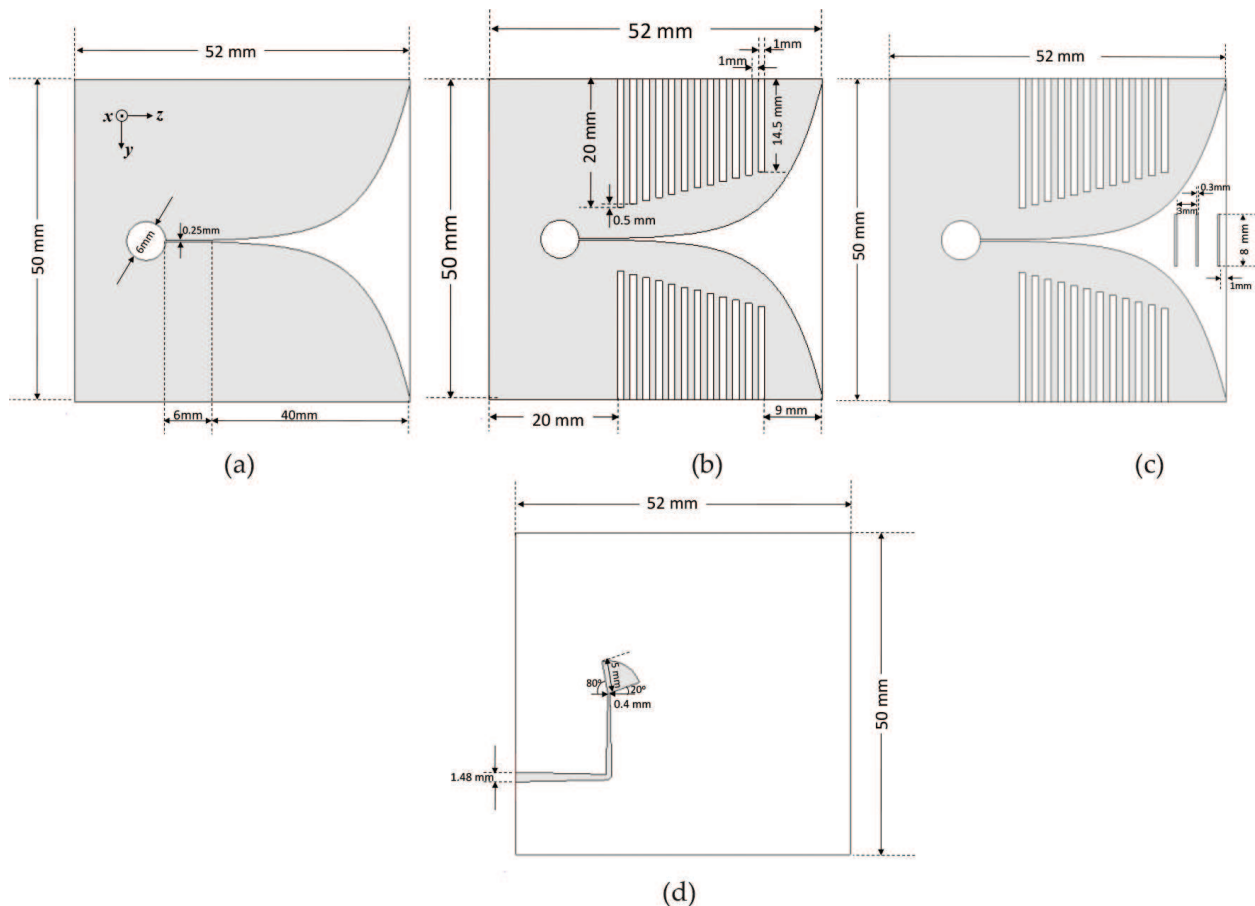


Figure 2. UWB Vivaldi antennas with its dimensions: (a) top view of Vivaldi; (b) top view of Vivaldi with corrugation; (c) top view of Vivaldi with corrugation and strip; (d) bottom view.

located to the flaring are the distance between strips, the width of strips and the length of strips. They are optimized as 3, 0.3 and 8 mm, respectively. All of the three Vivaldi designs use the same exponential tapering and balun. To match the antenna over a wide frequency band, a microstrip line to slot line transition and feed balun is designed as shown in **Figure 2d**. The selected reference axis system is also presented. The overall size of the antenna is not affected by the techniques used to increase the gain and improve the radiation patterns of the antenna in bore sight direction; therefore, the overall size of the antenna remains compact.

3.2. Antenna performance

To demonstrate the pulse distortion properties of the modified Vivaldi antennas, the prototypes have been manufactured with printed circuit board technology. The prototypes are shown in **Figures 1 and 3** (Vivaldi with corrugation and Vivaldi with corrugation and strip in **Figure 1**, standard Vivaldi in **Figure 3**). The scattering parameters of the antenna are measured using an Agilent vector network analyzer. The reflection behavior of each antenna has been investigated in terms of S_{11} . The measured return loss variation of the antennas is given in **Figure 4**. Simulations performed with a commercial finite integration technique-based software package computer simulation technology (CST) microwave studio, not reported for brevity, are in excellent agreement with the measurement results.

Simulated gain variations of the antennas are given in **Figure 5**. The realized gain of the modified antennas improves significantly throughout the frequency band compared to standard Vivaldi. Existence of the corrugations and grating elements maximizes the radiation in the bore sight direction. With the corrugations added, at the lower frequencies of the band, both of the modified Vivaldi antennas have higher gain compared to standard Vivaldi antenna. Moreover, Vivaldi with corrugation and strip has a 0.2 dB more gain than Vivaldi with corrugation at the whole frequency band. With these results, the positive effect of the existence of corrugation and metallic strips is observed in the frequency domain. However, since the antennas are aimed to be used for UWB applications, their time-domain performance should also be investigated.



Figure 3. Fabricated Vivaldi antenna (a) top view; (b) back view.

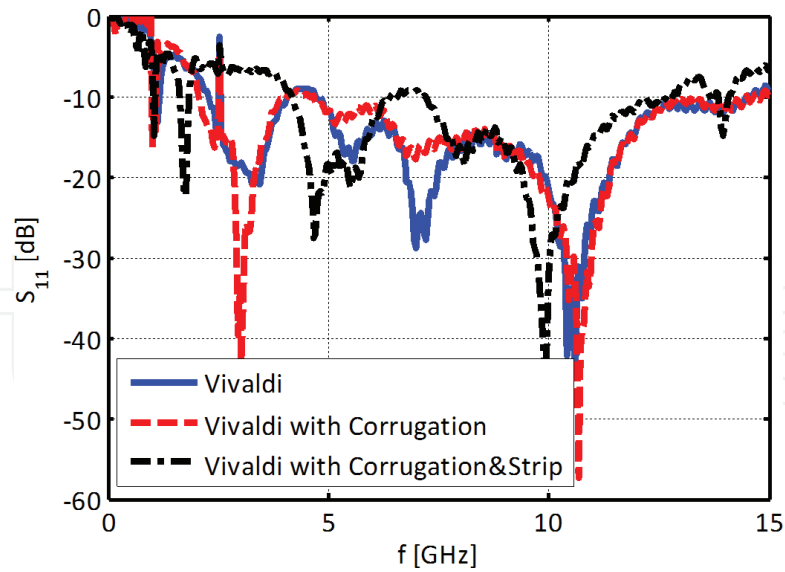


Figure 4. Measured return loss of Vivaldi antennas.

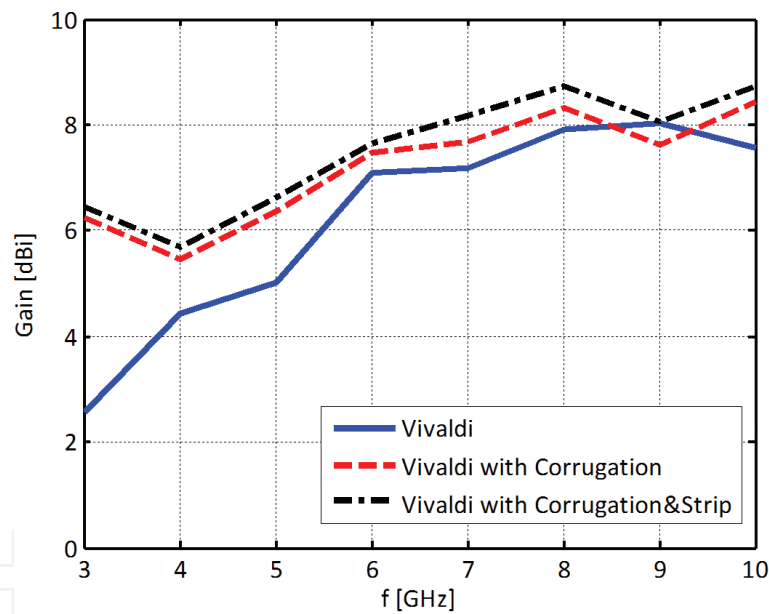


Figure 5. Simulated gain variations of Vivaldi antennas.

4. Time-domain analysis of modified Vivaldi antennas

4.1. Measurement setup

Time-domain analysis of modified Vivaldi antennas is performed and compared with that of standard Vivaldi antenna. A link composed of two identical Vivaldi antennas has been experimentally characterized. The measurements were performed with the same setup. The transmit-receive antenna link measurement setup demonstration for E-plane is shown in **Figure 6**.

The antennas were placed at about 20 cm of distance. In **Figure 7**, measurement setup is shown for E and H planes. In **Figure 8**, the amplitudes of S_{21} parameters at $\theta = 0^\circ$ are plotted as the function of the frequency in the range 0–12 GHz.

The procedure for the measurement of $S_{21}(\omega, \theta, \varphi)$ with angular variation can be summarized as follows: The measurements are performed by shifting one of the antennas in the range of $-90^\circ \leq \theta \leq 90^\circ$ with 5° steps in E- ($\varphi = 90^\circ$) and H-planes ($\varphi = 0^\circ$) and measuring $S_{21}(\omega, \theta, \varphi)$. Afterward, the impulse response of the link with angular variation is derived by means of inverse Fourier transform of the measured S_{21} as shown in the next section.

4.2. Time-domain analysis

4.2.1. Pulse comparison

The link between the transmitting and receiving antennas can be characterized in terms of its complex transfer function:

$$H(\omega) = U_{RX}(\omega)/U_{TX}(\omega) \quad (6)$$

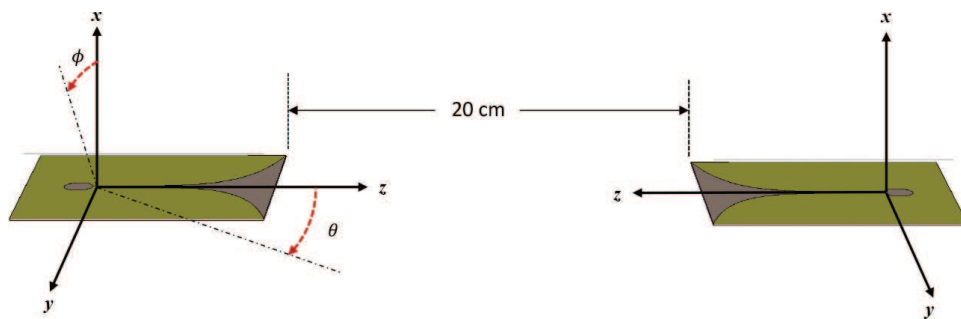


Figure 6. Demonstration of the measurement setup.

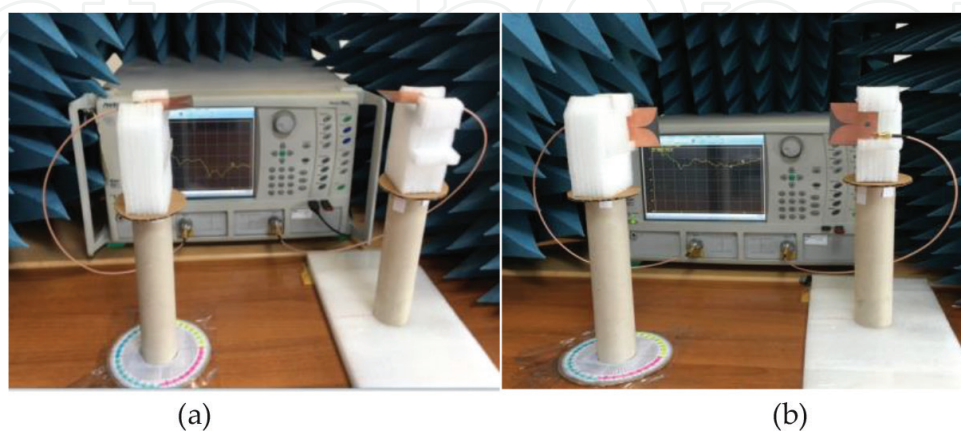


Figure 7. Measurement setup for the characterization of the antenna link (a) E-plane; (b) H-plane.

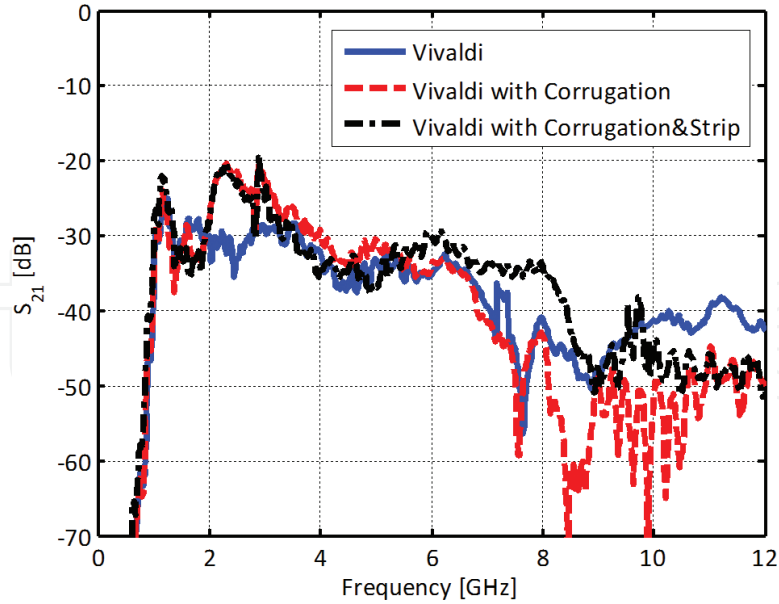


Figure 8. Measured insertion loss of the antennas.

where $U_{RX}(\omega)$ and $U_{TX}(\omega)$ are the spectra of the received and transmitted voltages, respectively. The coupling parameter between the antennas is related with the complex transfer function of the antennas as [22]:

$$S_{21}(\omega) = H_{TX}(\omega) H_{RX}(\omega) \frac{j\omega}{2\pi r c} e^{-j\omega r/c} \quad (7)$$

where $H_{TX}(\omega)$ and $H_{RX}(\omega)$ are the transfer functions of transmit and receive antenna. r is the distance between the antennas. The impulse response of the links is derived over 7.5 GHz bandwidth, from 3.1 to 10.6 GHz, by means of the inverse fourier transform (IFT) of the measured $S_{21}(\omega)$. In the application of time-domain analysis, the reference signal $S_{ref}(t)$ will be a sinc pulse associated with the mentioned 7.5 GHz band, which can be expressed as:

$$S_{ref}(t) = IFT\{S_{ref}(\omega)\} = \frac{1}{2\pi} \int_{\omega_1}^{\omega_2} e^{-j\omega t} d\omega \quad (8)$$

where $\omega_1 = 2\pi f_1$ and $\omega_2 = 2\pi f_2$. In Figure 9a-d, a comparison between the response of the antenna link in time domain and the reference signal delayed to the present maximum in correspondence of the main peak of the link's impulse response is shown for $\theta = 0, 10, 30, 45^\circ$ in the E-plane ($\varphi = 90^\circ$). The green dash-dot line is the ideal delayed pulse obtained by Eq. (8). Blue solid, red-dashed and black dash-dot lines belong to impulse response of the Vivaldi, Vivaldi with corrugation and Vivaldi with corrugation and strip, respectively. For a rigorous comparison, path loss effect is removed by scaling the received pulse amplitude to the transmitted amplitude. Thus, in the time-domain representations, the amplitude of the s_{21} parameter measured with the setup in Figure 7 is normalized to its maximum. The length of the coaxial cables used between the connector of the antenna and network analyzer

port is 50 cm. The Teflon coaxial cables for the transmitter/receiver antennas correspond to 4.83 ns of propagation time. The signal path in the microstrip antenna is 65.2 mm. With an effective dielectric constant of 1.97 at 5 GHz, the propagation time inside transmitter/receiver antennas are calculated approximately as 0.61 ns. A total of 20 cm free space propagation corresponds to 0.666 ns of propagation time. When the 2 cm adapters used at the network analyzer ports are added, total propagation time of the signal can be calculated as approximately 6.3 ns. This is observed from the time-domain representations obtained from the measurement results as well. The main peak of the signal arrives to the receiver after approximately 6.3 ns.

The half power width of the reference signal is 0.119 ns. When the antenna is at bore sight, half power width of the pulse for standard Vivaldi is measured as 0.011 ns wider than that of the reference signal. Similarly, the pulse is 0.076 and 0.03 ns wider for Vivaldi with

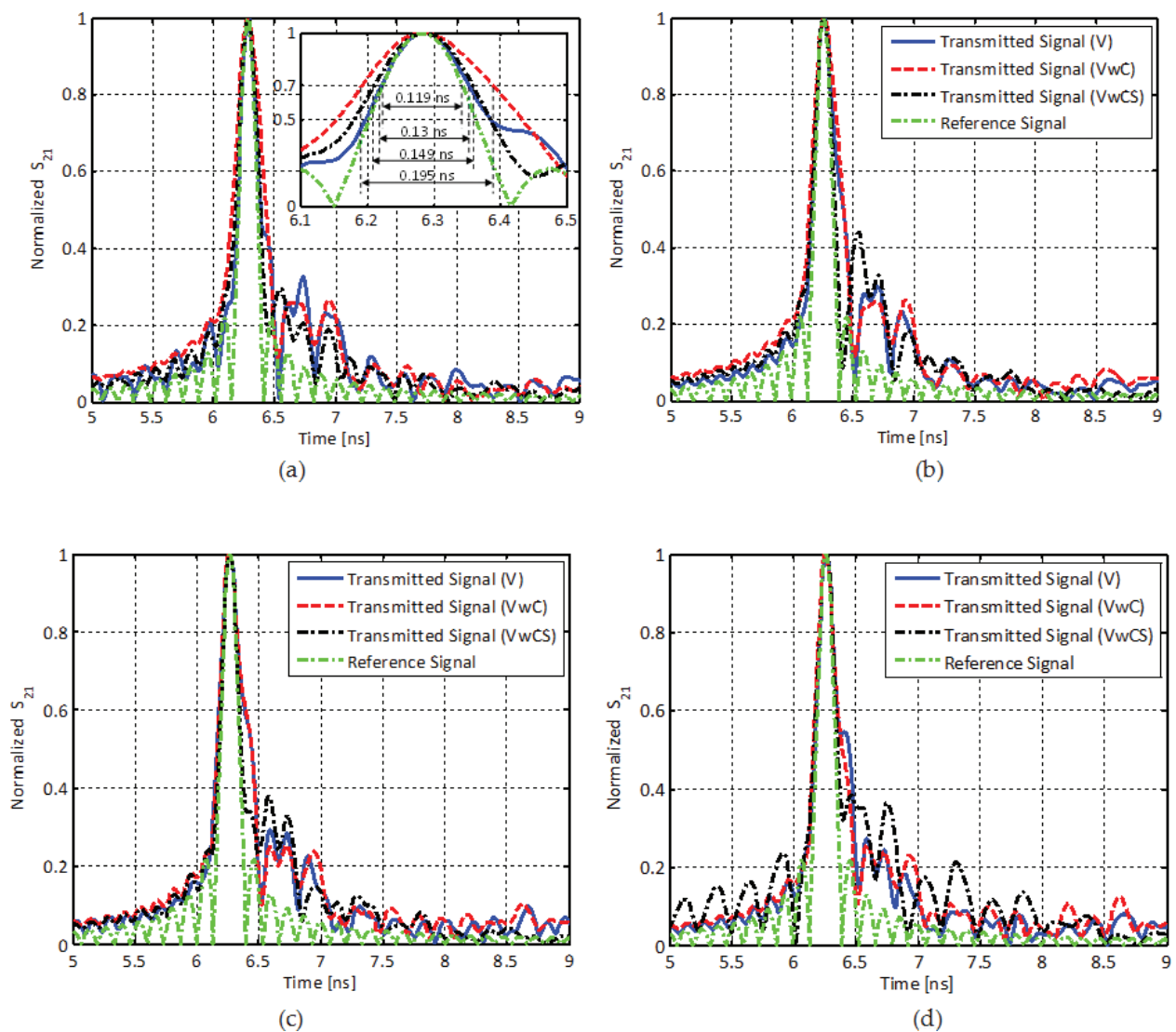


Figure 9. Comparison between the impulse response and an ideal delayed pulse in E-plane (a) $\theta = 0^\circ$; (b) $\theta = 10^\circ$; (c) $\theta = 30^\circ$; (d) $\theta = 45^\circ$.

corrugation and Vivaldi with corrugation and strip, respectively. The pulse is visible in the inset (**Figure 9a**). The pulses widen for larger values of θ . This is observed in **Figure 9b–d**. When $\theta = 0^\circ$ in E-field, the shape of the transmitted pulse is close to that of standard Vivaldi and Vivaldi with corrugation and strip. As theta gets larger, the pulses widen. This is observed at $\theta = 10^\circ$ given in **Figure 9b**. At 10° the main beam of Vivaldi with corrugation and strip pulse is similar to the main beam of reference pulse but secondary pulses are generated. A very similar case occurs at $\theta = 30^\circ$. At $\theta = 45^\circ$, secondary pulse of the standard Vivaldi is also generated.

Similarly, a comparison in H-plane ($\varphi = 0^\circ$) between the time-domain response of the antenna link that consists of standard Vivaldi and modified Vivaldi antennas and the reference signal, delayed by 6.3 ns to present the maximum in correspondence of the main peak of the link impulse response, is shown in **Figure 10**. In H-plane, pulse characteristics are different than the E-plane. Clearly, the pulse-preserving capability of Vivaldi with corrugation and strip is

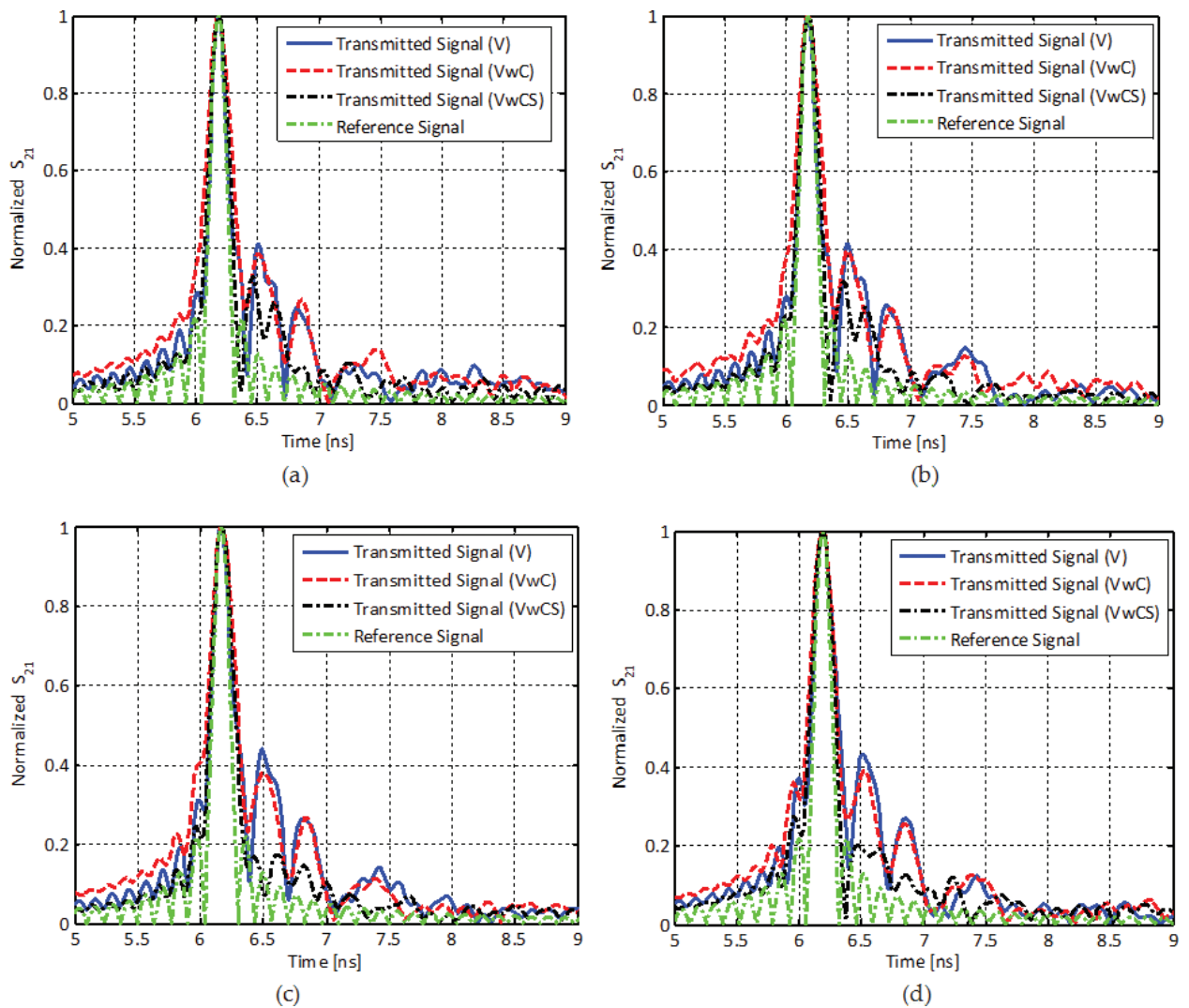


Figure 10. Comparison between the impulse response and an ideal delayed pulse in H-plane (a) $\theta = 0^\circ$; (b) $\theta = 10^\circ$; (c) $\theta = 30^\circ$; (d) $\theta = 45^\circ$.

better than the other Vivaldi antennas. Although only the measurement results are shared in this communication, simulations performed with CST, not reported for brevity, are in very good agreement with the measured results.

4.2.2. Pulse analysis

Based on the comparison between the impulse response of link and ideal delayed signal, one can clearly establish the presence of pulse widening. To quantify the amount of widening, pulse analysis with respect to θ in E- and H-planes are performed using the definition given in Eq. (3). In **Figure 11(a)** and **(b)**, half power width of the impulse response, τ is demonstrated in E- and H-planes, respectively. The green dotted line shows the width of the reference pulse which is equal to 0.119 ns.

Secondary pulse signal that has its maximum reach to half power of the main beam is generated by the link after 65° in E-plane and 70° in H-plane. As a result, pulse width is observed between $-65^\circ \leq \theta \leq 65^\circ$ for E-plane and $-70^\circ \leq \theta \leq 70^\circ$ in H-plane. Based on the pulse width results, it can be concluded that the width of the pulse that belongs to Vivaldi with corrugation widens more than the standard and corrugation and strip Vivaldi. This is valid both in E- and in H-planes. This result is even more obvious when the pulse width is compared to that of the reference signal. In **Figure 12**, pulse extension ratio of the measured pulse is given. It is calculated by the following expression:

$$\text{Pulse Extension Ratio} = \frac{\tau_{\text{pulse}} - \tau_{\text{reference pulse}}}{\tau_{\text{reference pulse}}} \quad (9)$$

The pulse extension ratio of Vivaldi with corrugation is below 65% in $-60^\circ \leq \theta \leq 60^\circ$. It goes above 100% afterward. Pulse width ratio of Vivaldi and Vivaldi with corrugation and strip is more stable than Vivaldi with corrugation. Based on pulse analysis results, one can accept the standard Vivaldi to have the best pulse distortion performance in the time

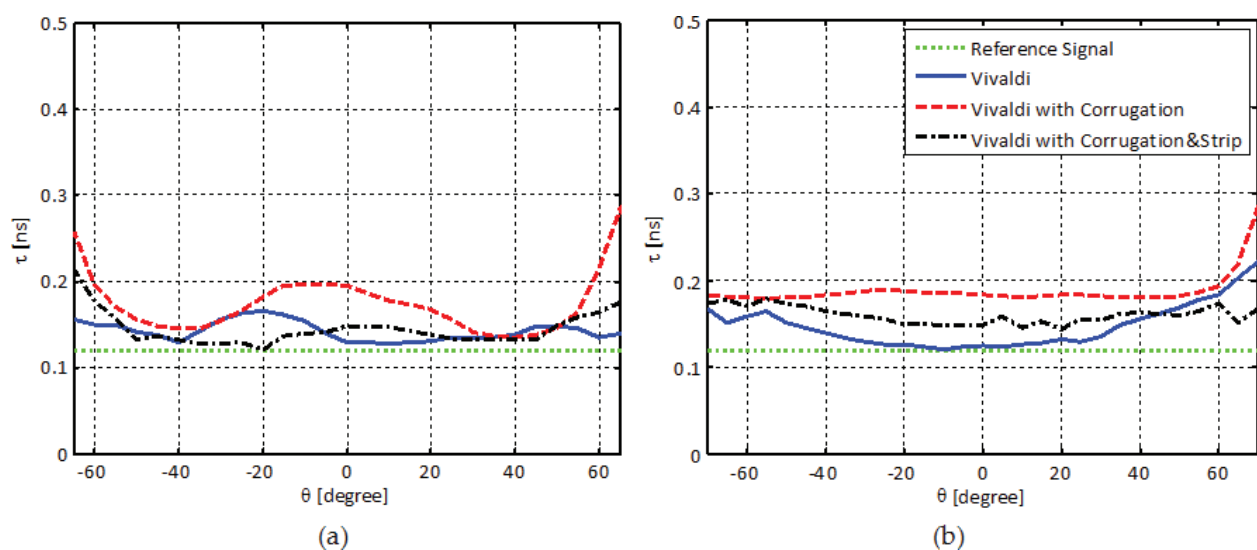


Figure 11. Half power width of the measured pulse (a) E-plane; (b) H-plane.

domain. Although, these results give an idea about the pulse distortion introduced by the Vivaldi antennas, to more rigorously quantify the pulse, distortion fidelity analysis should be performed.

4.2.3. Fidelity analysis

Most of the energy carried by the pulse is stored around the peak of the impulse. The correlation coefficient between the received pulse and transmitted pulse quantifies the similarity between transmitted and received signal. For the 3.1–10.6 GHz band, the fidelity factor of the link between two identical antennas is shown in **Figure 13** for E- and H-planes. The fidelity variation obtained from the measured S_{21} has unexpected pits at some angles. This may be due to the structure of the antenna profile. The fidelity values in E-plane are mostly close to 0.9 in

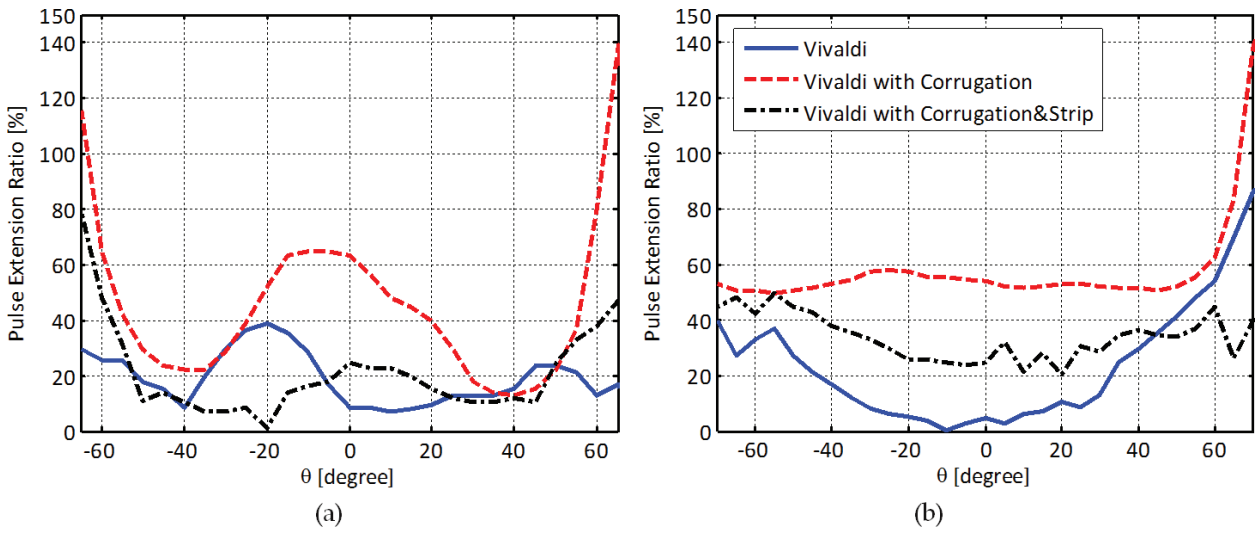


Figure 12. Pulse extension ratio of the measured pulse in (a) E-plane; (b) H-plane.

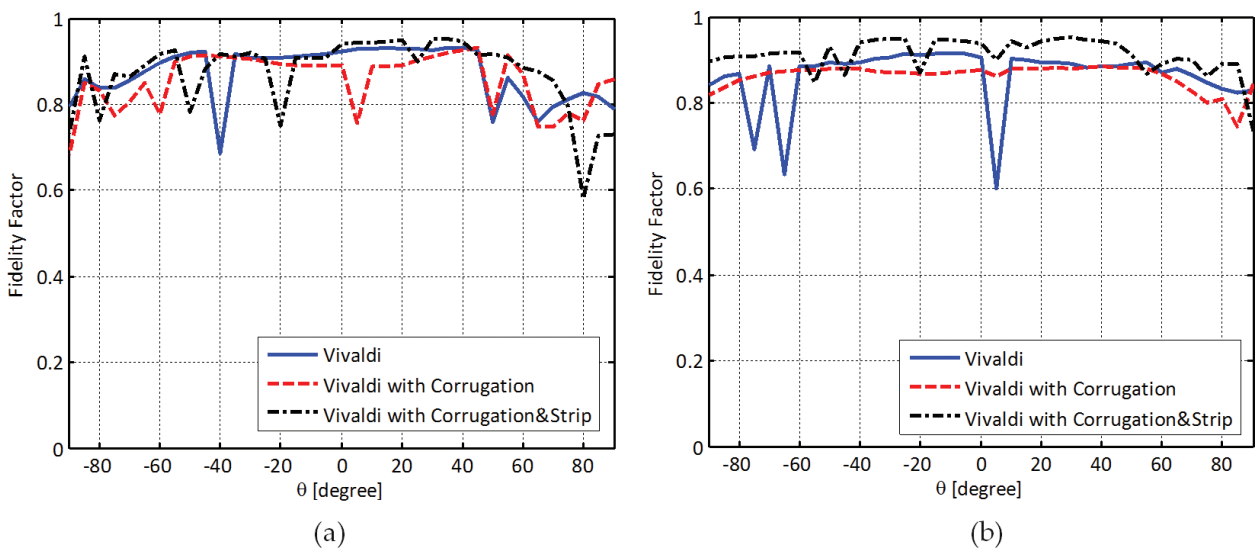


Figure 13. Fidelity factor variations of the pulses (a) E-plane; (b) H-plane.

for $-45^\circ \leq \theta \leq 45^\circ$. It has a lower value for the angles greater than 45° . In H-plane, Vivaldi with corrugation and strip has clearly a higher fidelity value than the others. Although standard Vivaldi was considered to have better impulse response in terms of pulse widening, fidelity analysis results represent Vivaldi with corrugation and strip to have the highest similarity between the transmitted and received signal. A good antenna performance requires simultaneously both a high fidelity and small pulse extension ratio of the impulse response. Thus, the modified version of Vivaldi antenna having corrugation and strip is a good candidate for UWB applications with its higher gain and wider bandwidth in the frequency domain and better pulse-preserving properties in the time domain.

5. Conclusion

In this chapter, the analysis procedure for the pulse-preserving properties of impulse-radiating antennas is defined. The analysis procedure is applied to a widely used UWB antenna, namely Vivaldi antenna. Vivaldi antennas are popular in UWB applications due to its complete planar structure which enables it to be easily integrated to UWB sensor circuit. However, Vivaldi antenna has relatively low directivity, especially at lower frequencies of the band. The lower frequency response of Vivaldi antennas may be improved by increasing the aperture size of the antenna. In the cases where physical size matters slots are added on the edges of exponential flaring to effectively increase the aperture of the antenna. The corrugated profile results in more suitable characteristics (i.e., higher gain, higher directivity, broader bandwidth). Besides adding slots on the edges of the flaring, adding grating elements on the slot area in the direction of the antenna axis is another technique to enhance the gain of the antenna. With the combination of both the corrugations and grating elements, the gain of the antenna increases significantly in the end-fire direction. Although these modified Vivaldi antennas are used in many UWB applications, their time-domain performance is not observed. With this contribution, pulse-preserving capabilities of modified Vivaldi antennas based on measurements are observed. Two parameters are used to quantify the capability of the antenna. First one is the pulse width extension that defines the broadening of the signal at its half power. Since most of the energy is stored around the peak of the pulse, this parameter is useful to demonstrate the pulse-preserving capability of the antenna but not sufficient. The second parameter is the fidelity factor that measures the correlation between the transmitted and received pulse. The performance of the modified Vivaldi antennas is also analyzed in different angular directions with respect to the main beam. Among the Vivaldi structures observed, Vivaldi antenna with corrugation and strip is proved to be potentially suited for both pulsed and harmonic broadband instruments.

Acknowledgements

This work was supported by Research Fund of the Yıldız Technical University (Project Number: FBA-2017-3071).

Author details

Sultan Aldırmaz Çolak¹ and Nurhan Türker Tokan^{2*}

*Address all correspondence to: nurhanturker@gmail.com

1 Department of Electronics and Communications Engineering, Kocaeli University, Kocaeli, Turkey

2 Department of Electronics and Communications Engineering, Yildiz Technical University, Istanbul, Turkey

References

- [1] Schwarz U, Thiel F, Seifert F, Stephan R, Hein MA. Ultrawideband antennas for magnetic resonance imaging navigator techniques. *IEEE Transactions on Antennas and Propagation*. 2010;**58**:2107-2112. DOI: 10.1109/TAP.2010.2046848
- [2] Chahat N, Zhadobov M, Sauleau R, Ito KA. Compact UWB antenna for on-body applications. *IEEE Transactions on Antennas and Propagation*. 2011;**59**:1123-1131. DOI: 10.1109/TAP.2011.2109361
- [3] Ardenne A, Smolders B, Hampson G. Active adaptive antennas for radio astronomy; results of the initial R&D program toward the square kilometer array. In: *Proceedings of the SPIE Conference 4015 Radio Telescope, Munich; March 27-30 2000*
- [4] "First report and order," Revision of Part 15 of the Commission's Rules Regarding Ultra-Wideband Transmission Systems Federal Communications Commission; 2002
- [5] Pancera E, Zwick T, Wiesbeck W. Spherical fidelity patterns of UWB antennas. *IEEE Transactions on Antennas and Propagation*. 2011;**59**:2111-2119. DOI: 10.1109/TAP.2011.2143666
- [6] Shlivinsky A, Heyman E, Kastner R. Antenna characterization in the time domain. *IEEE Transactions on Antennas and Propagation*. 1997;**45**:1140-1149. DOI: 10.1109/8.596907
- [7] Wiesbeck W, Adamiuk G, Sturm C. Basic properties and design principles of UWB antennas. *Proceedings of the IEEE*. 2009;**97**:372-385
- [8] Yang Y, Wang BZ, Ding S. Performance comparison with different antenna properties in time reversal ultra-wideband communications for sensor system applications. *Sensors*. 2018;**18**:88. DOI: 10.3390/s18010088
- [9] Gibson PJ. The Vivaldi aerial. In: *Proceedings of 9th European Microwave Conference, Brighton; September 17-20, 1979*. pp 101-105
- [10] Tokan NT. Performance of Vivaldi antennas in reflector feed applications. *Applied Computational Electromagnetics Society Journal*. 2013;**8**:802-808

- [11] Nassar IT, Weller TM. A novel method for improving antipodal Vivaldi antenna performance. *IEEE Transactions on Antennas and Propagation*. 2015;**63**:3321-3324
- [12] Oliveira AMD, Perotoni MB, Kofuji ST, Justo JF. A palm tree antipodal Vivaldi antenna with exponential slot edge for improved radiation pattern. *IEEE Antennas and Wireless Propagation Letters*. 2015;**14**:1334-1337. DOI: 10.1109/LAWP.2015.2404875
- [13] Wang YW, Wang GM, Zong BF. Directivity improvement of Vivaldi antenna using double-slot structure. *IEEE Antennas and Wireless Propagation Letters*. 2013;**12**:1380-1383. DOI: 10.1109/LAWP.2013.2285182
- [14] Zhang Y, ChaoWang EL, Guo G. Radiation enhanced Vivaldi antenna with double-antipodal structure. *IEEE Antennas and Wireless Propagation Letters*. 2017;**16**:561-564. DOI: 10.1109/LAWP.2016.2588882
- [15] Pandey GK, Singh HS, Bharti PK, Pandey A, Meshram MK. High gain Vivaldi antenna for radar and microwave imaging applications. *International Journal of Signal Processing Systems*. 2015;**3**:35-39. DOI: 10.12720/ijsp.3.1.35-39
- [16] Mehdipour A, Mohammadpour-Aghdam K, Faraji-Dana R. Complete dispersion analysis of Vivaldi antenna for ultra wide band applications. *Progress in Electromagnetics Research*. 2007;**77**:85-96. DOI: 10.2528/PIER07072904
- [17] Pancera E. Strategies for time domain characterization of UWB components and systems [Thesis] Universität Karlsruhe (TH) Fakultät für Elektrotechnik und Informationstechnik, Germany; 2009
- [18] Do-Hoon K. Effect of antenna gain and group delay variations on pulse-preserving capabilities of ultra wideband antennas. *IEEE Transactions on Antennas and Propagation*. 2006;**54**(8):2208-2215. DOI: 10.1109/TAP.2006.879189
- [19] Tokan NT, Neto A, Tokan F, Cavallo D. Comparative study on pulse distortion and phase aberration of directive ultra-wide band antennas. *IET Microwaves, Antennas and Propagation*. 2013;**7**(12):1021-1026. DOI: 10.1049/iet-map.2013.0032
- [20] Gopikrishnan G, Akhterand Z, Jaleel Akhtar M. A novel corrugated four slot Vivaldi antenna loaded with metamaterial cells for microwave imaging. In: *Proceeding of the Asia-Pacific Microwave Conference (APMC)*, New Delhi; 2016. pp. 1-4
- [21] Abbak M, Akıncı MN, Çayören M, Akduman L. Experimental microwave imaging with a novel corrugated Vivaldi antenna. *IEEE Transactions on Antennas and Propagation*. 2017;**65**:3302-3307. DOI: 10.1109/TAP.2017.2670228
- [22] Neto A. UWB, non dispersive radiation from the planarly fed leaky lens antenna. Part 1: Theory and design. *IEEE Transactions on Antennas and Propagation*. 2010;**58**:2238-2247

